The Potential of Low-Frequency SAR Systems for Mapping Ionospheric TEC Distributions

Franz Meyer, *Member, IEEE*, Richard Bamler, *Fellow, IEEE*, Norbert Jakowski, and Thomas Fritz

***Abstract*—Ionospheric propagation effects have a significant impact on the signal properties of low-frequency synthetic aperture radar (SAR) systems. Range delay, interferometric phase bias, range defocusing, and Faraday rotation are the most prominent ones. All the effects are a function of the so-called total electron content (TEC). Methods based on two-frequency global positioning system observations allow measuring TEC in the ionosphere with coarse spatial resolution only. In this letter, the potential of broadband L-band SAR systems for ionospheric TEC mapping is studied. As a basis, the dispersive nature of the ionosphere and its effects on broadband microwave radiation are theoretically derived and analyzed. It is shown that phase advance and group delay can be measured by interferometric and correlation techniques, respectively. The achievable accuracy suffices in mapping small-scale ionospheric TEC disturbances. A differential TEC estimator that separates ionospheric from tropospheric contributions is proposed.**

***Index Terms*—Atmospheric effects, correlation, dispersive media, ionosphere, L-band SAR, SAR interferometry, synthetic aperture radar (SAR), total electron content (TEC).**

I. Introduction

SMALL-SCALE turbulence phenomena in the ionosphere are still scarcely studied. This is mainly due to the lack of instruments and techniques capable of measuring these effects in an operational manner. As L-band synthetic aperture radar (SAR) systems are sensitive to ionospheric influences, we propose to use these effects for estimating the ionospheric state from L-band SAR by model inversion. In this letter, we will focus on the detectability of small-scale ionospheric structures in L-band SAR images. We propose three different algorithms for measuring different ionospheric target quantities.

All calculations are illustrated using a reference L-band SAR system that is similar to TerraSAR-L (see Table I). If we assume that the ionosphere is condensed to a thin layer at an altitude of 400 km, then the length of the system's synthetic aperture at the height of the ionosphere is about 8 km. To prevent signal blurring due to ionospheric turbulence of correlation lengths shorter than the synthetic aperture, we will use only one out of an arbitrary number of azimuth looks for processing. To get convenient numbers for the calculations in Section IV, we divide the synthetic aperture into eight independent looks. Later in the text, we will see that this is a reasonable number.

Manuscript received February 17, 2006; revised July 15, 2006.

F. Meyer and R. Bamler are with the German Aerospace Center (DLR), 82234 Wessling, Germany and also with Technical University Munich, 80333 Munich, Germany (e-mail: franz.meyer@dlr.de; richard.bamler@dlr.de).

N. Jakowski is with the German Aerospace Center (DLR), 17235 Neustrelitz, Germany (e-mail: norbert.jakowski@dlr.de).

T. Fritz is with the German Aerospace Center (DLR), 82234 Wessling, Germany (e-mail: thomas.fritz@dlr.de).

Digital Object Identifier 10.1109/LGRS.2006.882148

TABLE I
PARAMETERS OF THE L-BAND SAR REFERENCE SYSTEM

orbit height	H	800 km
carrier frequency	f_0	1.257 GHz
range bandwidth	B_r	80 MHz
antenna length	L_{ra}	14 m
synthetic aperture length in orbit	$L_{sa,orbit}$	16 km
synthetic aperture length in ionosphere	$L_{sa,iono}$	8 km
number of looks	N	8
length of look in orbit	L_{orbit}	2 km
length of look in ionosphere	L_{iono}	1 km
slant range resolution	ρ_{sr}	1.8 m
ground range resolution @ 30°	ρ_{gr}	3.6 m
cross-track resolution in ionosphere	$\rho_{gr,iono}$	1.8 m

II. Ionosphere

In the ionosphere, highly energetic solar radiation leads to the ionization of some atmospheric molecules and creates a mixture of free electrons, ions, and neutral gases. The density of free electrons n_e is a function of the sun's activity, atmospheric density profile, geographic location, magnitude and orientation of the Earth's magnetic field, and time of day. The electron density n_e increases with decreasing altitude, reaching a maximum at an altitude of about 250–400 km. Below this height, n_e quickly drops, as the radiation of the sun is more and more absorbed. Due to its shape, the barycenter of the electron density profile is situated above its maximum and is usually assumed to have a height of 400 km. Thus, a reference height of 400 km is used in global positioning system (GPS) practice to map total electron content (TEC) data from the slant to the vertical and vice versa.

If we treat ionized gas as a perfect dielectric, its refractive index for a radar wave of frequency f is given by

$$n_{\text{iono}} = \sqrt{1 - \frac{e_l^2}{4\pi^2 m \epsilon_0}\frac{n_e}{f^2}} \approx \left(1 - \frac{1}{2}\frac{e_l^2}{4\pi^2 m \epsilon_0}\frac{n_e}{f^2}\right) = 1 - K\frac{n_e}{f^2}\left(= 1 - \frac{f_c^2}{f^2}\right) \quad (1)$$

where $K = 40.28\ (\text{m}^3/\text{s}^2)$, e_l is the elementary charge, m is the electron mass, and ϵ_0 is the dielectric permittivity of vacuum. Equation (1) shows that the refractive index is a function of n_e. Note that the refractive index is smaller than unity and strongly depends on frequency. Thus, electromagnetic signals traversing through the ionosphere are "dispersively" delayed along their path, depending on the number of free electrons.

The deviation of the refractive index in the ionosphere from unity is small under normal atmospheric conditions; thus, the scaled-up "refractivity" N_{iono} is often used, instead of n_{iono}, i.e.,

$$N_{\text{iono}} = (n_{\text{iono}} - 1) \cdot 10^6 = -K \cdot 10^6 \frac{n_e}{f^2}. \quad (2)$$

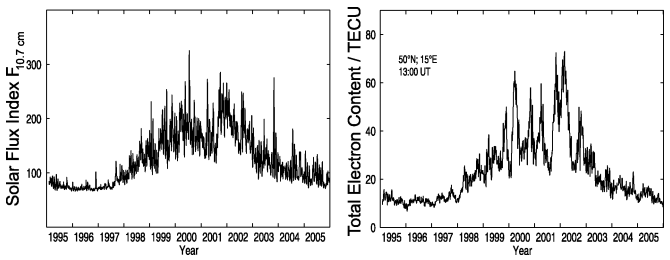

Fig. 1. Temporal variation of the daytime vertical electron content at the geographic site 50° N, 15° E during the last 11 years. The TEC data have been derived from GPS measurements obtained from the European receiver network of the International GPS Service [6].

As we show later in the text, it is convenient to use the column density of free electrons for analyzing the ionosphere's wave propagation properties. Thus, TEC $= \int_0^H n_e dh$ is usually used to describe the ionospheric state. The TEC values of the ionosphere are spatially and temporally highly variable [1], [2]. For European latitudes, TEC values may vary from very few free electrons to 100×10^{16} m^{-2} and more, depending on solar activity and the time of day. To calculate with convenient quantities, "TEC units" $(1 \cdot \text{TECU} = 1 \times 10^{16}$ m$^{-2})$ are usually used, instead of the original TEC values.

Besides variations of large spatial scale, additional small-scale disturbances of n_e exist. Such ionospheric irregularities predominantly occur at both equatorial and high latitudes. The spatial scales of disturbances reach from a few meters up to several hundred kilometers. Their magnitude is relatively small and is below 1 TECU for small-scale structures (smaller than 10 km) [3]. Within the extent of a SAR image, small-scale structures will mainly have measurable effects other than an offset. In [4], the so-called azimuth streaking effects, which are sometimes observed in SAR images of polar regions, are attributed to high-frequency ionospheric turbulence. Similar effects have been presented in [5].

The variation in daytime TEC values over the last 11 years is shown in Fig. 1 for a mid-European location (50° N, 15° E) in comparison to the corresponding 10.7-cm solar-flux index $F_{10.7\ \text{cm}}$ [Fig. 1 (upper panel)]. The daytime TEC values, which have been averaged over seven days to smooth day-to-day variability, show a close correlation with the solar-flux index. Besides its dependence on solar activity, a significant seasonal variation in TEC is also visible.

III. Ionospheric Effects on Broadband SAR Signals

A. Pulse Delay and Phase Advance

The effect of the ionosphere on a traversing SAR signal is that of an all-pass filter: every monochromatic signal component experiences a frequency-dependent phase shift.

For a nadir-looking radar, the two-way phase shift of frequency f compared to the propagation in vacuum is given by

$$\phi(f) = -2\pi f \frac{2}{10^6} \int_0^H \frac{N_{\text{iono}}(f,h)}{c} dh \approx 2\pi \frac{2K}{cf} \text{TEC} \qquad (3)$$

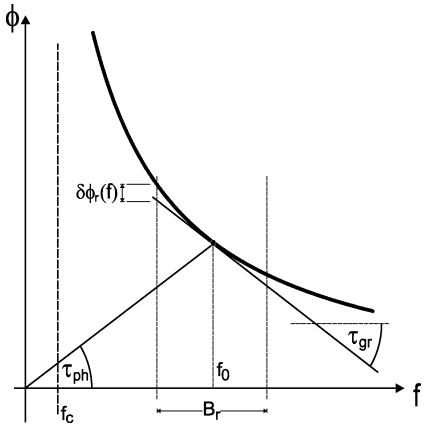

Fig. 2. Phase behavior of the ionosphere and its parametrization by phase delay τ_{ph}, group delay τ_{gr}, and residual phase curvature $\delta\phi_r(f)$. The traversing signal has the bandwidth B_r centered on center frequency f_0.

with c the vacuum speed of light. From (3), the phase delay

$$\tau_{\text{ph}} = -\frac{\phi(f_0)}{2\pi f_0} \approx -\frac{2K}{cf_0^2} \text{TEC} \qquad (4)$$

and the group delay

$$\tau_{\text{gr}} = -\frac{1}{2\pi} \left. \frac{d\phi(f)}{df} \right|_{f=f_0} \approx \frac{2K}{cf_0^2} \text{TEC} \qquad (5)$$

at radar center frequency f_0 can be derived. Equations (4) and (5) can be readily transformed into range delays by multiplication with 2/c. For a typical nonnadir-looking SAR, these equations must be multiplied by a geometry-dependent factor M to map from vertical to slant columns.

Fig. 2 schematically shows the phase behavior of the ionosphere, together with its relation to phase delay τ_{ph} and group delay τ_{gr}. The phase delay is negative. It describes the "advance" of the "phase" of the radar carrier. The (positive) group delay corresponds to the "delay" of the "envelope" of the (range-compressed) radar signal. Note that from (4) and (5), $\tau_{\text{gr}} \approx -\tau_{\text{ph}}$. The carrier phase and envelope experience a mutual shift that is caused by the ionosphere. Additionally, residual nonlinear phase distortions $\delta\phi_r(f)$ (Fig. 2) may blur the radar signal.

B. Effects in the SAR Image

1) Phase Advance: Spatially varying TEC distributions introduce phase errors in the SAR raw data. The resulting effects can be grouped into the following three classes.

1) TEC distributions of spatial wavelength much larger than the SAR image size result in a macroscopic phase screen in the focused image, resembling a slope in the range direction. The slope is caused by the range-dependent signal-path length through the ionosphere.
2) Inhomogeneities of medium spatial wavelengths may cause "phase gradients" across the azimuth chirp, which result in an azimuth shift of objects in the focused image. These effects, which are dubbed "azimuth streaks," were originally reported in [7] and were attributed to ionospheric effects the first time in [4].
3) Small-scale electron-density inhomogeneities across the synthetic-aperture length that cause quick phase

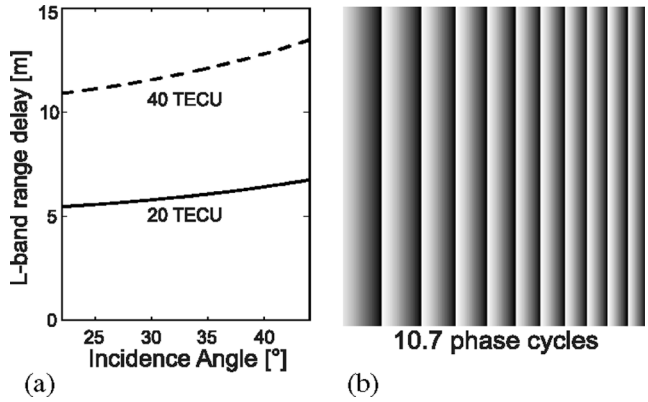

Fig. 3. (a) Range delay for two SAR acquisitions with ionospheric states of 20 and 40 TECU, respectively. The differential range delay amounts to more than 5 m. (b) Interferometric phase resulting from a TEC difference of 20 TECU. The simulation parameters are taken from Table I.

fluctuations will result in a decrease of the along-track resolution of a SAR.

Besides the aforementioned effects, small-scale TEC variations will cause additional phase distortions within a focused image. Hence, $\tau_{\rm ph}$ is the quantity to be considered for all interferometric applications. In [8], ionospheric phase screens are addressed and analyzed in detail, and a method for first-order correction of such screens is proposed. This method derives an estimate for the ionospheric phase contribution from the ionosphere-induced azimuth shift.

2) Group Delay: Constant TEC values across the SAR image cause a "macroscopic" range error of the SAR signal envelope. Spatial TEC variations lead to local geometric distortions of the focused SAR image and will affect coregistration with maps or other SAR images. Temporal TEC variations will lead to differential range shifts between multitemporal SAR images.

3) Nonlinear Phase Term: The residual phase function in the received signal that is not modeled by linearization via $\tau_{\rm ph}$ and $\tau_{\rm gr}$ is denoted by $\delta\phi_r(f)$ and is indicated in Fig. 2. $\delta\phi_r(f)$ is approximately quadratic and can be described by

$$\delta\phi_r(f) \approx \frac{4\pi}{c_0}\frac{K}{f_0^3}\mathrm{TEC}(f-f_0)^2. \tag{6}$$

This residual phase term results in a blur of the range impulse response function. For our reference L-band system, the residual quadratic phase at the margins of the range bandwidth is as low as 0.78° per TECU.

The following examples show the sensitivity of our reference L-band system to the aforementioned imaging effects. In the first step, we assume constant ionospheric properties across the whole SAR image in order to investigate the effects of a stable ionosphere on L-band SAR. Fig. 3(a) shows the incidence-angle-dependent ionospheric path delay of (5) for our reference system, assuming a 250-km-wide swath. It can be seen that an L-band SAR signal traversing an ionosphere with a spatially constant vertical electron content of 20 TECU experiences a (one-way) range delay of about 5.5 m in near range and about 7 m in far range, which is far beyond usual orbit accuracies. According to (5), this scales up to twice the delay and twice the range slope for a 40-TECU ionospheric state. The differential phase delay between two acquisitions with an ionospheric states of 20 and 40 TECU, respectively, gives rise to a residual phase ramp in range in an interferogram formed from these two images [see Fig. 3(b)]. The ionospheric-induced residual phase ramp accounts for 11 fringes for this configuration. Differential TEC values of 20 TECU and more between two images are likely to occur if they are acquired during different stages of the solar cycle (compare Fig. 1).

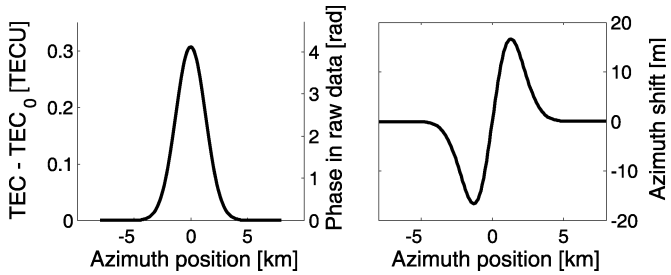

Fig. 4. Simulated ionospheric anomaly associated with its corresponding azimuth shift.

To determine the sensitivity of a TerraSAR-L-like SAR system to TEC fluctuations of short spatial extent, we assume a Gaussian TEC anomaly. To develop an anomaly model that matches typical ionospheric fluctuations, we considered observations of azimuth streaks published in [4]. According to these observations, a typical anomaly may have an amplitude of about 0.3 TECU and a width of 5 km. A schematic sketch of the simulated ionospheric anomaly and the associated azimuth shift calculated for our reference system is shown in Fig. 4. The shift reaches up to $\pm$20 m.

Higher order phase components of the ionospheric anomaly across the synthetic-aperture length may decrease the image resolution. Considering a single-look ionospheric-aperture length of 1 km, the maximal quadratic phase error $\delta\phi_x$ at the margins of the azimuth chirp, which is caused by this TEC disturbance, corresponds to approximately $\delta\phi_x = 0.1\pi$. This residual phase will not significantly decrease the along-track resolution of the SAR image.

C. Faraday Rotation

Most existing spaceborne SAR systems are equipped with linearly polarized SARs, which are affected by Faraday rotation [9]. The plane of polarization is rotated depending on the Earth's magnetic field, the ionospheric TEC, and the geometry of observation. Besides SAR polarimetry, Faraday rotation may also affect SAR interferometry if the two contributing images are acquired during different ionospheric states. The effects of Faraday rotation on SAR interferometry are discussed in detail in [10]. Faraday rotation effects can be removed from the data if fully polarimetric measurements are available. Some approaches are presented in [11].

IV. Measuring the Ionospheric State by SAR

The effects imposed by the ionosphere on L-band SAR images are usually considered nuisance, and the common treatment is to try to mitigate them in the data. Our approach is to make use of the high sensitivity of L-band SAR systems for estimating the ionospheric electron content (TEC), the differential TEC (ΔTEC) between two acquisitions, and the corresponding $d\Delta\mathrm{TEC}/dx$ azimuth gradient. In the succeeding subsections, some approaches that are capable of fulfilling this

TABLE II
IONOSPHERIC QUANTITIES THAT CAN BE ESTIMATED FROM SAR OBSERVATIONS, TOGETHER WITH THE EXPLOITED EFFECTS

Target quantity	Effects to be used
TEC	Blurring of range pulse due to residual phase
ΔTEC	Differential range shift Difference between phase and group velocity
$d\Delta TEC/dx$	Look misregistration Differential azimuth shift

task are introduced, and their applicability is evaluated. Table II gives a short overview of the target quantities, together with the effects that are exploited for their estimation.

A. Measuring Absolute TEC

If no external information is available as reference, absolute TEC measurements can only be made based on the quadratic residual phase term of (6). A variety of methods for estimating quadratic residual phase aberrations in SAR data is described in the literature. They are referred to as "autofocus algorithms." The most prominent are "blind deconvolution," "look correlation," and "phase-gradient autofocus." SAR systems comparable to our reference system show low sensitivity regarding the electron density in the ionosphere. Using the degradation of the peak power of a point scatterer as a measure for impulse-response blurring shows that a degradation to half the peak power is reached for a TEC level of nearly 200 TECU. A level of 200 TECU is extraordinarily high and only occurs during strong electromagnetic storms. Thus, an estimation of absolute TEC from L-band SAR data is not feasible in most cases.

B. Measuring Differential TEC

As demonstrated in Section IV-A, an "absolute" TEC map cannot be reliably derived from L-band SAR data. Nevertheless, in this section, we will show that L-band SAR systems have high potential for deriving "differential" TEC distributions ΔTEC, i.e., the difference of the ionospheric states between two SAR acquisition instances. A difference in TEC distribution gives rise to a differential group delay $\Delta\tau_{\mathrm{gr}}^{\mathrm{iono}}$ and a differential phase delay $\Delta\tau_{\mathrm{ph}}^{\mathrm{iono}}$ that map into mutual azimuth and range shifts as well as phase differences (see Sections III-A and B).

1) Estimator: Let a SAR system acquire two images of the same area, which are ideally from identical orbits, yet at different times. With sufficient temporal coherence assumed, we first compute a disparity map by correlation methods. The resulting vector field consists of estimates of the local range displacement Δr and the azimuth displacement Δx for every node on a predefined grid. These displacements are related to the aforementioned group and phase delays as well as to tropospheric delays $\Delta\tau^{\mathrm{tropo}}$ via

$$\frac{2}{c}\Delta r = \Delta\tau_{\mathrm{gr}}^{\mathrm{iono}} + \Delta\tau^{\mathrm{tropo}} \tag{7}$$

and

$$\frac{2}{c}\Delta x = \alpha\cdot\frac{d}{dx}\Delta\tau_{\mathrm{ph}}^{\mathrm{iono}} \approx -\alpha\cdot\frac{d}{dx}\Delta\tau_{\mathrm{gr}}^{\mathrm{iono}}. \tag{8}$$

In (8), α is a system- and geometry-dependent factor. Both equations are based on the assumption that the differential (nondispersive) tropospheric delay is mainly introduced by the lower troposphere. Hence, a gradient in tropospheric delay will not distort the phase of the azimuth chirp and can therefore be neglected.

As a second map, we compute the unwrapped interferometric phase $\Delta\phi$ between the two images, comprising the following information:

$$\frac{\Delta\phi}{2\pi f_0} = \Delta\tau_{\mathrm{ph}}^{\mathrm{iono}} + \Delta\tau^{\mathrm{tropo}} \approx -\Delta\tau_{\mathrm{gr}}^{\mathrm{iono}} + \Delta\tau^{\mathrm{tropo}} - m\cdot 2\pi \tag{9}$$

where m is the unknown integer phase cycle ambiguity unavoidable in interferometry. It is a single number for the entire interferogram.

None of the mentioned measures allows assessment of $\Delta\tau_{\mathrm{gr}}^{\mathrm{iono}}$ or $\Delta\tau_{\mathrm{ph}}^{\mathrm{iono}}$ directly. In order to obtain an estimate of the differential ionospheric group delay, which is proportional to differential TEC (ΔTEC), we compute the difference between the range displacement and interferometric phase measurements, i.e.,

$$\Delta\tau_{\mathrm{gr}}^{\mathrm{iono}} \approx \frac{1}{2}\left(\frac{2}{c}\Delta r - \frac{\Delta\phi + m2\pi}{2\pi f_0}\right). \tag{10}$$

According to (5), the final ΔTEC map is obtained from the group delay estimate by

$$\Delta\mathrm{TEC} \approx \frac{cf_0^2}{2K\cdot M}\Delta\tau_{\mathrm{gr}}^{\mathrm{iono}}. \tag{11}$$

Equation (11) only allows mapping of the spatially varying ΔTEC values. The long-wavelength ΔTEC components and hence the ambiguity number m may be derived from low-resolution TEC maps, as provided by GPS.

In addition, (8) allows an estimation of the differential TEC azimuth gradient $d\Delta\mathrm{TEC}/dx$ from Δx. This measure can be used together with (11) in an optimal estimation procedure and, by this, support an optimal solution.

2) Error Analysis: The main error contributions in (10) and (11) are the uncertainties in the correlation-based Δr estimation. The error of a shift estimation Δr by coherent cross correlation is analyzed in detail in [12], where its standard deviation is given by

$$\sigma_{\Delta r} = \sqrt{\frac{3}{2N}}\sqrt{\frac{1-\gamma^2}{\pi\gamma}}\cdot\rho_{\mathrm{sr}} \tag{12}$$

and is a function of the number of samples used N and coherence γ. For an average coherency of $\gamma = 0.5$, the differential range shift corresponds to $\sigma_{\Delta r} \approx (0.675/\sqrt{N})\cdot\rho_{\mathrm{sr}}$. From this, the standard deviation of the differential TEC estimate can be calculated via error propagation as

$$\sigma_{\Delta\mathrm{TEC}} = \frac{f_0^2}{2K\cdot M}\cdot\sigma_{\Delta r}. \tag{13}$$

Based on (12) and (13), the minimum number of samples, i.e., the final resolution of the TEC map required for achieving a predefined accuracy, can be found.

3) Example: From the anomaly model in Section III-B, it can be seen that typical small-scale ionospheric disturbances have magnitudes in the order of 0.3 TECU. Thus, an estimation accuracy of about 0.1 TECU is necessary for their detection.

In order to estimate TEC with this accuracy, the differential range shift between two SAR images must be measured with an accuracy of $\sigma_{\Delta r} = 5$ cm for the reference L-band system [see (13)]. Considering (12) and (13) and assuming a moderate interferometric coherence of $\gamma = 0.5$, the minimal number of samples $N_{\min}$ that is needed to reach the desired cross-correlation accuracy corresponds to

$$N_{\min} = \left(0.675 \frac{\rho_{\mathrm{sr}}}{\sigma_{\Delta r}}\right)^2. \tag{14}$$

Inserting the system parameters of Table I results in $N_{\min} \approx 590$. In order not to worsen the azimuth resolution of the theoretical SAR system (cf. Table I), only samples in range direction are used for correlation. Thus, 590 samples in range direction enable an estimation of differential TEC with an accuracy of $\sigma_{\Delta\mathrm{TEC}} \approx 0.1$ TECU. The spatial resolution of an ionospheric map derived with this approach is 1 km $\times$ 1 km if only one out of eight looks is used. If all eight independent looks are combined, the number of necessary samples can be reduced to $N_{\min} \approx 130$, and the spatial resolution of the TEC map improves to 1 km (azimuth) $\times$ 230 m (range).

In order to estimate differential TEC azimuth gradients $d\Delta\mathrm{TEC}/dx$, differential azimuth shifts Δx must be measured with sufficient accuracy. As shown in Section III-B, $d\Delta\mathrm{TEC}/dx$ may reach up to ± 20 m for typical TEC anomalies, which corresponds to about 0.3 multilooked resolution cells. This shift is easily detectable by cross-correlation procedures. Thus, an estimation of $d\Delta\mathrm{TEC}/dx$ is possible with high spatial resolution.

4) Practical Considerations: The proposed estimation schemes assume that the two interferometric acquisitions are taken from the same orbit, which is a requirement never met exactly in real systems. Hence, topography-induced disparities and phases must be compensated before estimating the ionospheric delay. If precise satellite orbits and a digital elevation model of the observed area are available, this problem is easy to solve.

As shown before, the wide beamwidths of L-band systems require the synthetic aperture to be split into shorter pieces, i.e., looks, for achieving a reasonable azimuth resolution in the ionospheric layer. Note that in this case, corresponding pixels in the different looks are affected by different parts of the ionosphere, as they are not observed from the same position along the orbit. Thus, if ionospheric TEC maps from different looks should be combined for achieving higher estimation accuracies, they have to be shifted against each other in azimuth. Fig. 5 shows how the estimates from different looks must be combined in order to "see" the same ionospheric cell. Note that this type of look processing reduces the influence of uncompensated tropospheric and topographic signals in addition.

V. Conclusion

The presence of the ionosphere has a significant impact on the measurement of all upcoming spaceborne L-band SAR systems and has to be considered in system design and data processing. The sensitivity of L-band SAR to changes in the ionospheric state and to ionospheric turbulence suggests its application for ionospheric mapping with high spatial resolution and high accuracy. Approaches for detecting and studying small-scale ionospheric structures have been presented, and their potential has been analyzed. In particular, ΔTEC and $d\Delta\mathrm{TEC}/dx$ can be estimated with high accuracy. Ground-based estimations of TEC using dense GPS networks such as GEONET can reach neither this accuracy nor a comparable spatial resolution due to the separation of radio links of several tens of kilometers on average. It should be noted that with a usual sun-synchronous orbit configuration, the temporal evolution of the ionospheric state will always be undersampled, as it is true for many atmospheric sounding missions. Although the temporal resolution of the proposed method cannot compete with ground-based measurements, it promises insights into ionospheric processes and related structures due to the high spatial resolution of TEC derivatives.

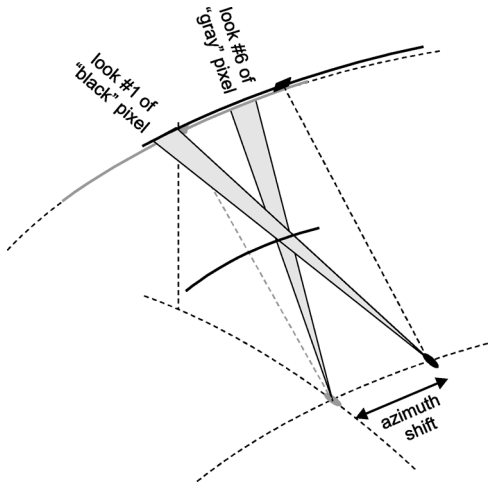

Fig. 5. How to combine ionospheric measurements from different looks by appropriate azimuth shifting.

References

[1] P. Snoeij, N. van der Valk, E. Boom, and D. Hoekman, "Effect of the ionosphere on P-band spaceborne SAR images," in *Proc. IGARSS*, Sydney, Australia, 2001, pp. 132–134.
[2] N. Jakowski, "Ionospheric GPS radio occulation measurements on board CHAMP," *GPS Solutions*, vol. 9, no. 2, pp. 88–95, Jul. 2005.
[3] A. Bhattacharyya, T. Beach, P. Basu, and P. Kintner, "Nighttime equatorial ionosphere: GPS scintillations and differential carrier phase fluctuations," *Radio Sci.*, vol. 35, no. 1, pp. 209–224, 2000.
[4] A. Gray, K. Mattar, and G. Sofko, "Influence of ionospheric electron density fluctuations on satellite radar interferometry," *Geophys. Res. Lett.*, vol. 27, no. 10, pp. 1451–1454, May 2000.
[5] S. Quegan and J. Lamont, "Ionospheric and tropospheric effects on synthetic aperture radar performance," *Int. J. Remote Sens.*, vol. 7, no. 4, pp. 525–539, 1986.
[6] N. Jakowski, "TEC monitoring by using satellite positioning systems," in *Modern Ionospheric Science*. Berlin, Germany: Produserv GmbH Verlagsservice, 1996, pp. 371–390.
[7] J. Joughin, D. Winebrenner, M. Fahnestock, R. Kwok, and W. Krabill, "Measurement of ice-sheet topography using satellite-radar interferometry," *J. Glaciol.*, vol. 42, no. 140, pp. 10–22, 1996.
[8] K. Mattar and A. Gray, "Reducing ionospheric electron density errors in satellite radar interferometry applications," *Can. J. Remote Sens.*, vol. 28, no. 4, pp. 593–600, 2002.
[9] M. Faraday, "On the magnetization of light and the illumination of magnetic lines of force," *Philos. Trans. R. Soc. London.*, vol. 136, no. 1, pp. 1–62, 1846.
[10] E. Rignot, "Effect of Faraday rotation on L-band interferometric and polarimetric synthetic-aperture radar data," *IEEE Trans. Geosci. Remote Sens.*, vol. 38, no. 1, pp. 383–390, Jan. 2000.
[11] A. Freeman, "Calibration of linearly polarized polarimetric SAR data subject to Faraday rotation," *IEEE Trans. Geosci. Remote Sens.*, vol. 42, no. 8, pp. 1617–1624, Aug. 2004.
[12] R. Bamler and M. Eineder, "Accuracy of differential shift estimation by correlation and split-bandwidth interferometry for wideband and Delta-k SAR systems," *IEEE Geosci. Remote Sens. Lett.*, vol. 2, no. 2, pp. 151–155, Apr. 2005.